

Sensitivity of γ -Ray Detectors to Polarization

I.-A. Yadigaroglu

Department of Physics, Stanford University, Stanford, CA 94305-4060

1. Introduction

The *EGRET* instrument aboard *CGRO* is the largest γ -ray detector to date and has collected several thousand photons above 30 MeV for the strongest sources, the Vela and Crab pulsars. Most of the energy output of young pulsars is in beamed γ rays which emission models predict to possess a high degree of linear polarization (*eg.* Romani and Yadigaroglu 1995), and polarization observations would prove a particularly potent probe of magnetospheric geometry and physics.

At γ -ray energies above a few MeV, photon interactions with matter are increasingly dominated by pair production. Detectors in this energy range thus observe the resulting e^+/e^- pair to reconstruct the original photon properties. When the incident γ -ray photon is polarized, the e^+/e^- azimuthal angles about the photon direction are initially correlated with the polarization position angle with a modulation factor $\sim 20\%$, and the potential for measuring polarization has long been recognized (Yang 1950, Wick 1950, Maximon and Olsen 1962). However, as pointed out first by Kel'ner *et al.* (1975), multiple scattering in the converting material and measurement errors *exponentially* suppress the final modulation factor. This is to be contrasted with detector angular resolution where the dependence on scattering and errors is linear. Instruments optimized to collect large numbers of photons with reasonable angular resolution will thus not be adequate to measure polarization.

For this reason, initial hopes of sensitivity to polarization for *COS B* and *EGRET* (*eg.* Kotov 1988, Caraveo *et al.* 1988) have not been confirmed by more detailed simulations and the analysis of actual event data (Mattox 1992, Mattox *et al.* 1990). Since then, the next generation γ -ray instrument *GLAST* has been proposed and sophisticated simulation software developed to analyze its future performance. Sufficient detail is included in the software model to confidently predict polarization sensitivity. As the *GLAST* design has not been finalized at this stage, quantitative studies such as the present one should be helpful in optimizing its performance for a variety of physics goals, including polarization measurements.



We summarize the principal features of the pair production cross section (§2) and current γ -ray instruments (§3). Simple estimates of the polarization modulation factors are derived (§4) and Monte Carlo simulations performed for a single conversion foil (§5). The details of particle reconstruction in multiple plane detectors are discussed (§6) along with our simulation results for *GLAST* (§7).

2. Pair Production Modulation Factors

Polarization can be measured only for bright sources so that the source position is well determined and the observed e^+/e^- pair events are completely described by six parameters: the photon energy ω_γ , the energy split ϵ^+ (or ϵ^-) between the positron and electron, and the four spherical angles about the known photon direction and an arbitrary position angle on the sky (from North through East is the usual convention): θ^+ , θ^- , ϕ^+ , and ϕ^- . The e^+/e^- fork will tend to lie in a plane that includes both the photon direction and its linear polarization vector, resulting in a modulation of the pair production cross section of the form:

$$\sigma_{\text{PP}} \propto 1 + \lambda \cos^2 \psi$$

where ψ is the azimuthal angle of the e^+/e^- plane and $\lambda \sim 1/3$ at high energies and when all production events are included. Some authors prefer to use a quadrupole signal of the form $1 + R \cos 2\psi$, where $\lambda = 2R/(1 - R)$, as the average of cosine is zero. If this property is desired, one can also use $1 + \Lambda (\cos^2 \psi - 1/2)$, where $\lambda = \Lambda/(1 - \Lambda/2)$. For partially polarized photons, both R and Λ (but not λ) are proportional to the amount of polarization.

The cross section topology is of course much richer than this simple integral shows, and ideally the information in the cross section should be used more fully in order to increase the sensitivity to polarization. When one looks for instance only at events where the energy of the photon is split equally between the electron and positron, λ increases to $2/3$ (averaged again over all other quantities). At lower photon energies $\omega_\gamma < 100$ MeV, λ also increases. For plots of λ as a function of several parameters see Kotov (1988).

In an approximate sense, it is useful to think of the physical process of pair production as creating the e^+/e^- pair exactly in the plane of polarization. The recoil momentum of the nucleus q then stochastically changes the azimuthal angle of the fork to random directions. Sets of events for which the nucleus recoil momentum is small thus have a larger value of Λ . Events with small q are much more likely since the

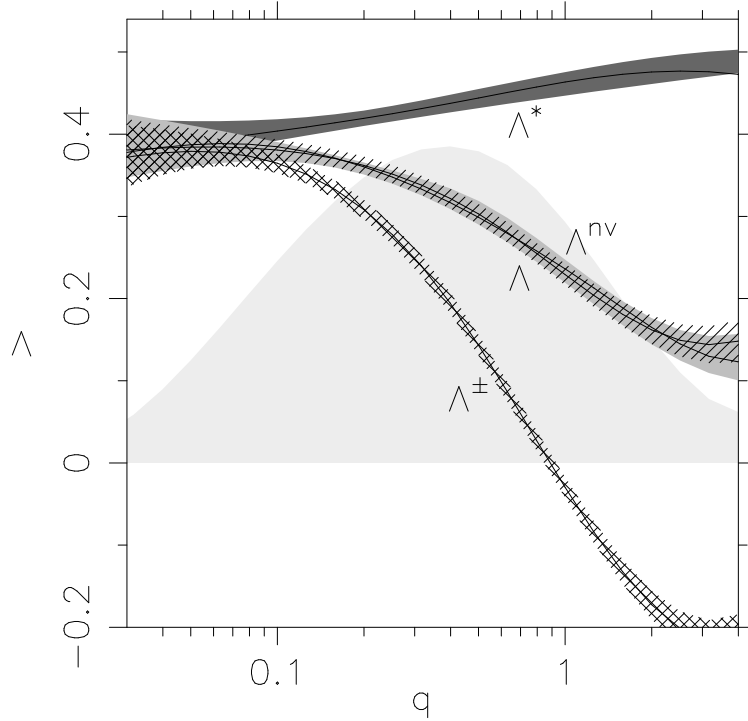


Figure 1. Polarization signal at $\omega_\gamma = 30$ MeV as a function of the nucleus recoil momentum q . The top curve (darkest) is the modulation amplitude Λ^* of ψ^* , the middle curve is for either Λ of ψ (lighter) or Λ^{nv} of ψ^{nv} (hatched), and the lower curve (cross-hatched) for Λ of ϕ^+ or ϕ^- (for which Λ can be multiplied by $\sqrt{2}$ as there are two possible measurements per event). Modulation is seen to vary from $\sim 40\%$ at zero momentum transfer, to negative values at large q for ϕ^\pm . The light region shows the number of events as a function of q in arbitrary units. The curves are based on 10^7 Monte Carlo events with statistical 1σ noise represented by the curve widths.

cross section includes a $1/q^4$ term; competing against this dependence is the vanishing phase space at zero momentum transfer q to the atom.

In constructing the azimuthal angle ψ of the e^+/e^- fork plane, the effect of the nucleus recoil momentum partially cancels. For this reason, the polarization modulation Λ of ψ is larger than that observed for the two azimuthal angles of the e^+/e^- tracks, ϕ^+ and ϕ^- . Of course one expects the modulation to be larger by a factor $\sqrt{2}$, as there are two possible measurements in the case of ϕ^\pm , and ψ is some average of ϕ^\pm . The angle ψ has, however, larger modulation than expected from a simple average of the ϕ^\pm . In fact, other weighted averages of the two angles ϕ^+ and $\phi^- \pm \pi$ are even more successful in cancelling the

coherent effects of the recoil momentum. The best we have found is:

$$\psi^* \equiv w^+ \cdot \phi^+ + w^- \cdot (\phi^- \pm \pi), \quad w^\pm = \frac{\sqrt{\epsilon^\pm \cdot \sin \theta^\pm}}{w^+ + w^-}$$

where π is added to or subtracted from ϕ^- depending on whether ϕ^+ is larger or smaller than ϕ^- , respectively (and with the branch cut $[0, \pi]$ for all angles). As seen in Figure 2, ψ^* is almost entirely successful at eliminating the dependence on recoil momentum. Unfortunately, as ψ^* depends also on θ^\pm (as does ψ), it is more difficult to measure than ϕ^\pm , so there will be a tradeoff between greater intrinsic modulation and increased measurement error. The inclusion of ϵ^\pm in the definition of ψ^* is not essential and results in only a small improvement of the measured modulation.

To determine the fork angles θ^\pm and ϕ^\pm , a minimum of three points is needed: the vertex of the pair production event and at least one measurement along each of the e^+/e^- tracks. If the vertex of the event is not measured, we are left with two points from which only a single azimuthal angle ψ^{nv} can be constructed. Since scattering in each measurement plane significantly perturbs the e^+/e^- tracks, ψ^{nv} may sometimes be the best estimator as it involves only one measurement plane. As can naively be expected, Figure 2 shows ψ^{nv} to possess the same degree of modulation as ψ .

3. Current Detector Designs

Pair production ceases to be the dominant conversion process below a critical photon energy $610 \text{ MeV}/(Z + 1.24)$, where Z is the atomic number of the conversion material (in gases the corresponding formula is $710 \text{ MeV}/(Z + 0.92)$). In addition, the resulting e^+/e^- pair must possess enough energy to create two distinct tracks in the detector. Both the *EGRET* and *GLAST* designs thus make use of many thin, high Z conversion foils, with as little material as needed for the active measurement planes and support structures sandwiched between them.

The *EGRET* instrument has 27 tantalum pair production foils of radiation thickness $\tau = 0.022$ separated by 16.6 mm for a total of about half a radiation length along 45 cm. In between the foils spark chambers measure the track x and y coordinates with wires spaced 8 mm apart. The lower portion of the detector has some additional spark chambers with only small amounts of scattering material in between, and two of these are rotated by 45° to help in resolving the ambiguity in pairing together x and y coordinates to form positions in the detector. The

EGRET effective area decreases rapidly below ~ 100 MeV and above a few GeV.

The current design of the *GLAST* instrument calls for 12 lead conversion foils of radiation thickness $\tau = 0.05$ separated by 30 mm for a total of about half a radiation length along 36 cm. Silicon strips with ~ 250 μm pitch just below the foils measure the track x and y coordinates. The amount of silicon in the strip planes is not negligible and amounts to a total of 0.0077 radiation lengths for the x and y planes, unless a single double-sided plane is used.

To limit the strip length, *GLAST* is made of modules, with some area lost between the modules. *GLAST* accepts photons from almost 2π of the sky, so that photons can have oblique incident angles to the foils. This larger acceptance combined with better triggering results in a much improved effective area for *GLAST* as compared to *EGRET*, especially at low energies. At 30 MeV *GLAST* should collect about 20 times more photons than *EGRET*. Below 30 MeV, the effective area remains much higher than that of earlier detectors, but drops rapidly to a small fraction of the geometric area.

4. Simple Estimates

As noted in the introduction, the polarization modulation factors are suppressed *exponentially* by measurement errors and multiple scattering, as is easily shown by integrating the quadrupole in “ ψ ” (any ψ or ϕ) with a Gaussian error of width σ_ψ (errors on ψ are of course defined modulo $\pi/2$). The quantitative decrease of “ Λ ” (again, any of the Λ ’s) can then be understood from some simple formulas. For an incident photon being measured a distance z from its conversion point, the error σ_ψ due to multiple scattering σ_θ and measurement error σ_{xy} is given by:

$$\sigma_\psi \approx \frac{\sigma(z)}{z \cdot \sin \theta}, \quad \sigma(z)^2 \equiv \sigma_{xy}^2 + (z \cdot \sigma_\theta(\tau, E))^2$$

A rough estimate of multiple scattering for $\tau = X/X_0$ radiation lengths traversed at energy E is given in Lynch and Dahl (1991):

$$\sigma_\theta(\tau, E) = \frac{13.6 \text{ MeV}}{E} \cdot \sqrt{\tau} (1 + 0.038 \cdot \log \tau)$$

For an ensemble of events at some particular energy, θ can be replaced with a characteristic polar angle $\langle \theta \rangle$ for the set. The median polar angles of the electron and positron vary strongly with energy. At 100 MeV, the median is 0.67° , and 2.2° at 30 MeV. In fact $\langle \theta \rangle \propto 1/E$

is a good approximation, where E can be either the photon energy ω_γ , or the individual energies ϵ^\pm of the e^+/e^- tracks. Inserting the expression for $\sigma(z)$ and assuming small $\langle \theta \rangle$ gives:

$$\sigma_\psi^2 \approx \left(\frac{\sigma_{xy}}{z \cdot \langle \theta \rangle} \right)^2 + \left(\frac{\sigma_\theta}{\langle \theta \rangle} \right)^2$$

If the measurement error σ_{xy} dominates the errors, low energies are clearly favored as $\langle \theta \rangle$ will be large (C is a constant):

$$\Lambda \propto \exp \left(-C \cdot \left(\frac{\sigma_{xy}}{z \cdot \langle \theta \rangle} \right)^2 \right) \approx \exp \left(-C \cdot \left(\frac{\sigma_{xy} \cdot E}{z} \right)^2 \right)$$

However, if multiple scattering dominates the errors, Λ decreases exponentially with τ and is independent of $\langle \theta \rangle$ or E :

$$\Lambda \propto \exp \left(-C \cdot \left(\frac{\sigma_\theta}{\langle \theta \rangle} \right)^2 \right) \approx \exp(-C \cdot \tau)$$

Photons can pair produce anywhere in the foil, so that in the scattering dominated case the polarization signal will be due to events that were produced close to the surface of the foil. The signal will then only decrease linearly with τ (since the fraction of events close to the surface will decrease linearly with thickness). We can thus expect exponential decrease followed by linear decrease of Λ for large τ . The last expression also reveals that there is little benefit in choosing individual e^+/e^- tracks with a high fraction of the photon energy in order to minimize the effects of scattering, since these will have on average correspondingly small polar angles (i.e. a plot of the ψ error as a function of ϵ^\pm is flat). Similarly, Λ does not depend strongly on ω_γ . Since most astronomical objects have a steep spectrum, polarization is again best measured at low energies.

To summarize, in the energy range where errors are dominated by scattering, all photons contribute equally to polarization sensitivity, and at higher energies, polarization modulation decreases exponentially. It does happen, however, that *particular* events are very good, and others very bad. Equal energy split with large opening angle is ideal. At the other extreme are events with no measurable opening angle, and thus no azimuthal angle information. A weighted histogram of the ψ can thus be calculated in finding Λ . It must be kept in mind though that assigning weights is analogous to making cuts on the events, and so the statistical noise is increased. The question then is whether there is sufficient gain in the signal amplitude to offset this increased noise.

5. Single Foil Results

The preceding section showed that polarization is best measured at the lowest possible photon energies. This explains the choice of $\omega_\gamma = 30$ MeV in Figure 2, since the *GLAST* effective area decreases rapidly at even lower energies. In this energy range, measurement of the e^+/e^- track angles is clearly dominated by multiple scattering. Even though the e^+/e^- tracks will often traverse many measurement planes, the later measurements will have little memory of the initial e^+/e^- fork angles. Before simulating a complete detector, it is thus useful to analyze the situation when only one production foil is involved, and under the assumption that the angles and energies of the e^+/e^- pair are measured perfectly after leaving the conversion foil. These best case results will present a benchmark for simulations of the complete detector.

In our simulations we have used the polarized pair production cross section σ_{PP} in the static field limit (no energy transfer to the nucleus) and without screening, as given in *eg.* Jauch & Rohrlich (1975). The main effect of screening is to change the total cross section which is not of interest here. We also neglect pair production on the electron field, and the effects of the Coulomb field of the e^+/e^- pair. We do not restrict ourselves to the limit of small momentum transfer as Maximon and Olsen (1962) have done. For multiple scattering we have used the expression of §4.

The simulation results for the different Λ are shown in Figure 5. The first panel shows the almost exponential decrease of the signal Λ with increasing foil thickness τ , and the second panel the optimal choice of τ that maximizes the signal to noise ratio for a single foil (or more generally for a fixed number of foils). The larger Λ at small τ is offset by the smaller number of photons that will convert in a thinner foil. The curves shown are for $(\tau/0.05) \times 10^5$ events (i.e. constant flux, and 10^5 conversions in a foil of thickness 0.05). The signal to noise ratio is seen to be relatively flat between $\tau = 0.001$ and 0.1. With no measurement errors, a 3σ observation would require only 8000 conversion events for foils with $\tau = 0.01$ (using ψ^*). The figure curves are smoothed versions of Monte Carlo sums of 5×10^5 events, spaced every 0.1 in $\log \tau$ (so twenty runs for each curve).

Both *EGRET* and *GLAST* measure x and y coordinates of the e^+/e^- tracks in separate active layers, and the pairing together of the x and y to form detector positions is not known when more than one track is recorded in the same layer. Resolving these ambiguities is essential to the measurement of polarization, since the azimuthal angles can change by $\sim 90^\circ$ when the wrong x and y are combined. In Figure 5 the corresponding loss of modulation is shown for the entire range from

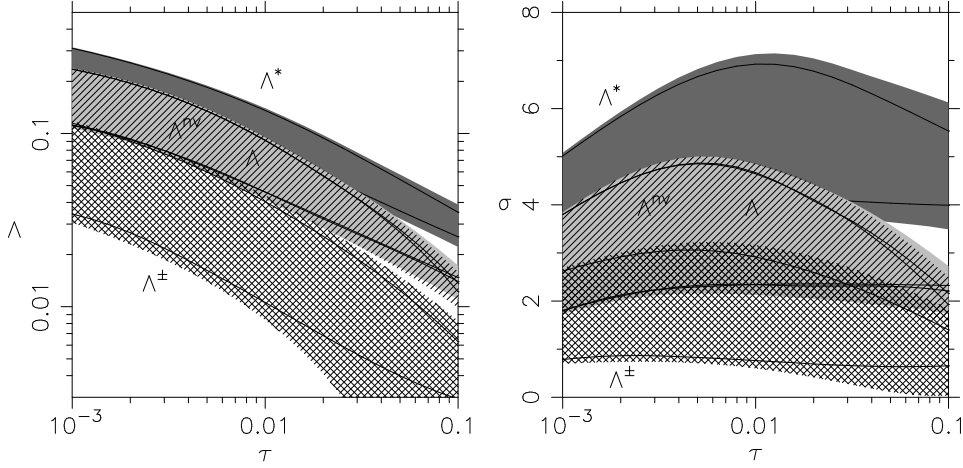


Figure 2. Results at $\omega_\gamma = 30$ MeV for a single foil and no measurement errors ($\sigma_{xy} = 0$). The first panel shows the close to exponential decrease of Λ with the foil thickness τ in radiation lengths. The curves are as in Figure 2, with the difference that the widths represent the loss in modulation expected from x/y pairing ambiguities in addition to the Monte Carlo 1σ noise. The second panel shows the corresponding signal to noise ratio in σ for $(\tau/0.05) \times 10^5$ photon conversions.

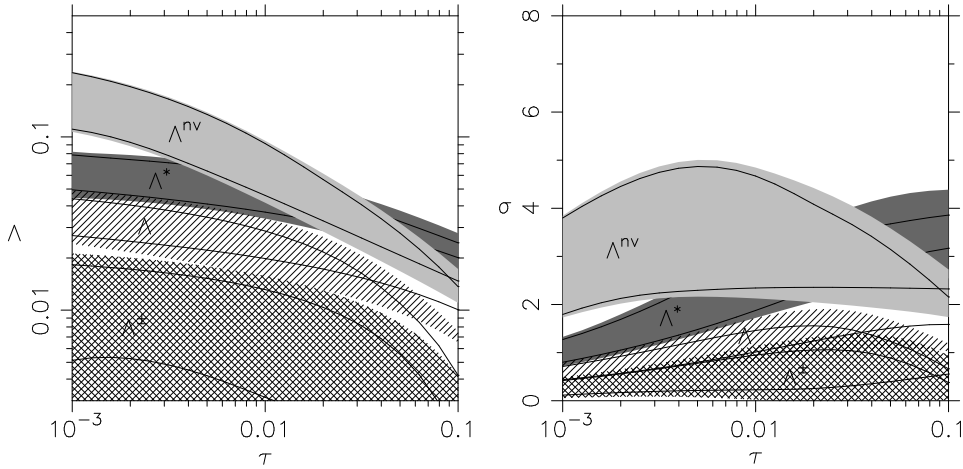


Figure 3. Addition of an active layer just below the conversion foil is needed to measure the event vertex. Scattering in this active layer reduces the modulation as compared to Figure 5. Here we have assumed an active layer 0.0077 radiation lengths thick (eg. 700 μm of silicon). Results for Λ^{nv} are copied from Figure 5 as no vertex need be measured in constructing ψ^{nv} .

no ambiguity to full ambiguity (i.e. from no errors, to bad pairing half of the time). With complete ambiguity, 25000 events are needed for a 3σ detection (factor 3 more). As is explained in section §7, some of this loss can be regained by assigning event weights.

As mentioned in §2, the event vertex must be measured in order to determine all four track angles. An active layer is thus required just below the conversion layer. A second active layer some distance away will then measure the track angles from the vertex position. Unfortunately, the tracks will also be scattered in the first active layer as they must traverse its entire thickness. In the case of *GLAST* the active layers have significant thickness, 0.0077 radiation lengths in the current design (two 350 μm layers of silicon). Figure 5 shows the dramatic decrease in modulation expected when scattering from the first active layer is included. The effect is most pronounced for thin conversion foils. In the case of ψ^{nv} no vertex is needed, and so the curves have been copied from Figure 5. For most of the τ range, ψ^{nv} now has larger modulation than ψ^* . For thinner active layers, this will not be the case.

An important effect was not included in Figure 5. If the active layer has significant thickness, additional photon conversions will take place in the active layer itself. These events will be highly modulated, as the relevant τ is now the active layer thickness, which is usually much less than the conversion foil thickness. There are several complications though. If enough energy is deposited in the active layer to allow measurement of the vertex, it is not possible to distinguish such an event from a conversion in the foils. In the contrary case, the event will not have a vertex and thus only ψ^{nv} can be constructed. When separate active planes are used to measure the x and y coordinates, the event will have both coordinates only half the time. Finally, as explained in §3, many conversions in the low Z active material are Compton events. Nevertheless, in the case of *GLAST*, $\tau = 0.05$ for the conversion foils and Figure 5 applies, and for the active layers, $\tau = 0.0077$ and Figure 5 applies. Depending on the importance of these effects and x/y ambiguities, photons that converted in the active layers may dominate the polarization signal. This will be discussed further in §7.

In the second panels of Figures 5 and 5, it was assumed the resulting modulation is of the form $\cos^2 \psi$, so that the signal to noise is given by $\Lambda/(0.028 \times \sqrt{N})$ for $N \times 10^4$ measurements of “ ψ ” (any ψ or ϕ^\pm). We have found that measuring an asymmetry ratio results in a slightly improved signal to noise as compared to fitting the $\cos^2 \psi$ modulation (approximately 10 % larger). Clearly the measured modulation is not described optimally by a \cos^2 and a better estimator should be derived. This was not investigated further.

The results for single foils are also useful in interpreting designs which are dominated by measurement errors and for which track angles are effectively measured only after traversing *several* foils. In this case the combined τ traversed is most relevant, and one simply regains the situation where scattering dominates after n foils have been traversed. The foil thickness is then $\tau \times n$. At 100 MeV, *EGRET* is dominated by measurement errors with $n \sim 4$.

6. Monte Carlo Simulation

To simulate the *GLAST* instrument in detail, we have used the standard *GLAST* Monte Carlo software which is an application built upon Gismo (Atwood *et al.* 1992). Gismo, written in C++, includes both QED interactions adapted from the EGS4 code and hadronic processes from the Gheisha code. The *GLAST* application includes many details of the detector geometry that can affect the instrument performance, for example, all materials with significant radiation length (converter planes, silicon-strip detectors, readout electronics, structural support elements, thermal control material), dead areas around the edges of each module, and gaps between modules. Energy deposition in the active portions of the silicon tracker and calorimeter is also modeled in detail, and only the simulated digital outputs are available to the event reconstruction classes.

We have modified the software in several important ways. First, the polarized cross section as described in §5 was added as a new interactor class. Second, the event reconstruction code was entirely rewritten. This was necessary since the standard reconstruction (simple linear fits through the tracker and calorimeter) is inadequate for low energy events. The requirements for polarization sensitivity are that individual e^+/e^- tracks and the production vertex be identified correctly, giving estimates of the track angles and energies from which the ψ , ψ^* or ψ^{nv} are constructed. Several approaches to event reconstruction were experimented with, but we have had the most success with a brute force search of all possible tracks through the silicon-strip detector.

The silicon tracker output is a list of x and y strip “hit” coordinates at given z heights. Our strategy is then to test all possible sequences of hit positions (x, y, z) , looking for downward (increasing z) sequences with as little scatter as possible. Writing the correct likelihood criterion for a track is a difficult problem and it depends on the entire tracker output, so that we have used an ad hoc expression instead:

$$\mathcal{L} \equiv \sum_i v_i - \sqrt{(n-2) \cdot \sum_i v_i^2 - (\sum_i v_i)^2}, \quad v_i \equiv 1 - \alpha_i^2,$$

where for a sequence of n foils, we have $(n - 2)$ scattering angles α_i (in radians). The second term of \mathcal{L} favors tracks for which the amount of scattering is constant along the track. A list of likely (large \mathcal{L}) tracks is built up during the recursive search, and saved tracks are replaced with more likely versions if they are judged to be similar enough (as defined by the direction of the tracks and the number of points common to both). We thus obtain a complete list of the best dissimilar tracks found. Several million possible sequences must be tested in this way and optimized algorithms from the GNU C++ library were used to allow the search to finish within a second for most events (Sun UltraSparc).

As explained in section §5, a complication is that the pairing together of x and y hit positions is not known when more than one hit is recorded by the tracker at a given z . All possible combinations are thus treated equally. This results in “real” tracks also having “shadow” tracks present in the final list. Resolving these ambiguities is important to the measurement of polarization, since we are interested in the track azimuthal angles. If a track crosses the boundaries of a module, the ambiguity is resolved automatically. Otherwise the limited imaging capability of the calorimeter must be combined with energy estimates from multiple scattering in finding the most likely “real” tracks. Individual track energy estimates are thus an important element in finding likely tracks. For our purposes a simple inversion of the Gaussian multiple scattering formula was found to be sufficient. With no measurement errors, the expected energy resolution is only $1/\sqrt{n - 2}$, where n is the number of foils traversed, so that for small n the estimate from scattering is useful only as a consistency check against the energy deposited in the calorimeter.

A second processing stage then takes the saved tracks as input and decides on the most likely combination of “real” tracks, using all the information available. A score is calculated for each combination that includes contributions due to: the ratio of energies estimated from scattering and from the calorimeter, the fraction of the total calorimeter energy assigned to tracks, the number of tracker hits used, the number of “shadow” hit pairs used, and the existence of a vertex. The highest score selects a particular set of tracks along with estimates of their individual angles and energies. Which tracks are “real” is of course most reliably determined close to the calorimeter, and we must follow the tracks back to the vertex in order to determine the original fork angles. As *GLAST* is entirely scattering dominated at low energies, only the vertex and next layer were used in calculating the e^+/e^- angles about the known incident photon direction. Otherwise, the next track positions would provide additional estimates of the angles.

7. Results and Discussion

In general terms, this reconstruction algorithm delivers close to optimal low energy response for *GLAST*. All but 7 % of the events which convert within the tracker are reconstructed (some are too complex to search in the allowed time or have no recognizable tracks), individual tracks are identified, and their energies determined to 20 % FWHM or better at 30 MeV. Almost half of the events are found to have two tracks with a well defined vertex. A single track is found for 30 % of the events; these correspond mainly to cases where the e^+/e^- energy split was asymmetric. Three or more tracks are found in the remaining 25 % of cases. Compared to the standard *GLAST* reconstruction, effective area is increased by more than 15 % at 30 MeV. In addition, angular resolution is also improved, in part by summing the track momenta to obtain the incident photon direction. The single photon angular resolution is 1.8° FWHM at 100 MeV, and 6° at 30 MeV.

The measured polarization sensitivity is, however, disappointing. From Table 1, one finds that, without modifications, the *GLAST* design would require 7×10^5 photon events for a 3σ detection of 100 % polarized flux. With the new reconstruction algorithm, the *GLAST* effective area is $\sim 7000 \text{ cm}^2$ at 100 MeV, and $\sim 5000 \text{ cm}^2$ at 30 MeV. For the Vela pulsar, *GLAST* will thus collect ~ 6000 counts/day above 100 MeV, and ~ 8000 counts/day in the range 30–100 MeV. A 3σ detection would thus require two months of observing time. Observations of ~ 20 % polarization in several phase bins would not be possible. Changes to the *GLAST* design in order to improve polarization sensitivity are clearly indicated.

In order to verify that the *GLAST* sums agree with the simple simulation described in §5, we simulated a single conversion foil with the *GLAST* code, using only two active layers: one directly below the conversion foil, and one at a large distance. The resolution of the active layers was arbitrarily good, and there was no x/y ambiguity. Table 1 shows the *GLAST* results to be comparable to the simple simulation, *eg.* Λ^* of 0.0449 compared to 0.0541. The simple form for multiple scattering (and the absence of Bhabha and Moller scattering) adopted in the simulations of §5 can easily account for these differences, since all errors affect λ exponentially. The Monte Carlo sums of Table 1 were all allowed to run for approximately 60 workstation days, resulting in several million events per configuration. Monte Carlo noise is then sufficiently small to make meaningful measurements of all “ Λ ” except Λ^\pm .

In going from a single conversion foil to the complete *GLAST* geometry, there is a further decrease in modulation, *eg.* from 0.0185 to

Table I. Polarization sensitivity at 30 MeV, for both the simple and detailed Monte Carlo sums. Single foil results are for Pb conversions, $\sigma_{xy} = 0$, and no x/y ambiguity. The required number of events / 10^3 for a 3σ detection is reported (100 % polarized flux). The number of events reflects both the modulation amplitude Λ and fraction of all reconstructed events used. The required exposure is thus given by the number of events / flux \times effective area. Results for $\cos^2 2\phi_0$ event weights are also shown, where ϕ_0 is the angle between the detector x axis and the polarization direction. Each Monte Carlo sum was run for approximately 60 workstation days, resulting in several million reconstructed events per run.

<i>Single foils</i>						
	foil τ	ψ	$\Lambda \times 100$	3σ		
Simple MC	0.05	ψ	2.70	77^{+25}_{-17}		
		ψ^*	5.41	19^{+3}_{-2}		
Si added for vertex	0.05 + 0.0077	ψ	1.12	448^{+509}_{-189}		
		ψ^*	3.33	51^{+13}_{-9}		
Detailed MC	0.05	ψ	2.26	140^{+141}_{-56}		
		ψ^*	4.49	36^{+13}_{-9}		
	0.05 + 0.0077	ψ	1.09	622^{+676}_{-258}		
		ψ^*	1.85	216^{+106}_{-61}		
	0.02 + 0.0038	ψ	1.64	258^{+170}_{-86}		
		ψ^*	4.31	37^{+7}_{-6}		
<i>Multiple Planes</i>						
	foil τ	ψ	$\Lambda \times 100$	3σ	$\Lambda \times 100$ \cos^2	3σ \cos^2
Standard <i>GLAST</i>	0.05 + 0.0077	ψ^*	0.90	865^{+318}_{-205}	1.16	725^{+238}_{-160}
		ψ^{nv}	0.89	2200^{+1519}_{-748}	1.35	1331^{+647}_{-375}
No x/y ambiguity		ψ^*	0.96	766^{+276}_{-179}		
		ψ^{nv}	1.87	499^{+138}_{-98}		
Double-sided Si	0.05 + 0.0038	ψ^*	0.87	909^{+444}_{-257}	1.17	700^{+288}_{-178}
Thin foils	0.02 + 0.0077	ψ^*	1.98	162^{+39}_{-29}	2.17	188^{+50}_{-36}
		ψ^{nv}	2.82	235^{+71}_{-49}	4.10	155^{+37}_{-27}
Double-sided Si	0.02 + 0.0038	ψ^*	2.90	75^{+17}_{-13}	3.22	84^{+21}_{-15}
Double-sided Si, no x/y		ψ^*	3.72	45^{+12}_{-9}		
		ψ^{nv}	7.11	49^{+14}_{-10}		
Rear Si	0.05 + 0.0077	ψ^{nv}	1.08	586^{+299}_{-170}	1.79	297^{+98}_{-65}
	0.02 + 0.0077	ψ^{nv}	2.43	129^{+55}_{-34}	3.37	93^{+33}_{-21}

0.0090 for Λ^* . This decrease must be due to a combination of x/y ambiguities and other reconstruction errors. Using our simple simulations as a guide, we expect the modulation to decrease by half when x/y ambiguities are present. Although the reconstruction algorithm correctly selects “real” tracks over “shadow” tracks, near the vertex we find that the position ambiguities are not well resolved since both “real” and “shadow” positions are closely clustered together. The error made by pairing the x and y coordinates incorrectly can be very different depending on the orientation of the instrument axes as compared to the original track azimuthal angle. The best situation is when the fork plane contains one of the axes so that there is no ambiguity, and the worst is when the axes are rotated by 45° from this position so that an incorrect pairing will give an error of 90° . The orientation of the e^+/e^- fork plane before scattering is of course not known, but the events can be weighted with $\cos^2 2\phi_0$, where ϕ_0 is the angle between the detector x axis and the assumed polarization direction. The modulation is increased in this way, *eg.* from 0.0090 to 0.0116 for Λ^* , and results in increased sensitivity to polarization.

The x/y ambiguities can be resolved directly by modifications to the *GLAST* design. For instance, if at least one strip layer per module is rotated by an angle 0° – 45° , x/y ambiguities can in principle be resolved. This complicates the module design as the strips are then of unequal length, and the readout electronics must also be mounted differently. The same result can also be achieved by correlating energy deposition in the x and y coordinates, or, for the last active layer, by adopting a calorimeter with better imaging capabilities, such as the proposed “Sci-Fi” design. The modulation signal from the last foil may approach in this case the optimal single foil value reported in Table 1, since both angles and individual track energies would be reliably measured. We have modified the *GLAST* code to eliminate x/y ambiguities. Results as given in Table 1. The effect is most dramatic for ψ^{nv} , where modulation is observed to more than double.

Returning to the standard *GLAST* design, the table also shows Λ^{nv} to be of the same magnitude as Λ^* . Unfortunately, in the initial layer, separate tracks can be resolved for very few events, as there is no separation between the conversion foil and first active layer. As a result, too few events are resolved to be useful for polarization. A simple modification of the *GLAST* design would be to separate the active layers from the conversion foils, contrary to the current design. The results for this modification are noted in the table with “Rear foils”. Rear foils are seen to improve the sensitivity to polarization by 50 %. Angular resolution at low energies is decreased though, from 1.8°

to 2.6° FWHM at 100 MeV; there is no such effect at high energies, as errors are dominated by the strip pitch.

A more promising modification of the *GLAST* design is to increase the number of conversion foils while decreasing their thickness, as now seems possible. The simple simulation of Figure 5 shows that halving the foil thickness should increase modulation by at least 50 %. We have simulated the case $\tau = 0.02$. Polarization modulation more than doubles, as can be seen from Table 1. A less drastic modification of the *GLAST* design would be to make the active Si layers thinner, since the scattering in the first active layer has a large effect on the modulation of ψ^* . Results for half the usual Si thickness (double-sided Si) are given in Table 1 and show that the modulation does not improve over the standard design. This surprising result can be explained from the arguments of §5. For $\tau = 0.05$ foils, Si events dominate the polarization sensitivity, and half of these events are lost with the decreased Si thickness.

Doubled-sided Si layers, i.e. with the x strips on one side, and the y strips on the other side of the same Si layer, are nevertheless desirable. When two separate layers are used, half of the events which convert in the Si will convert in the second layer and will thus have only one coordinate. These events are not useful for polarization measurements (although one then knows that the conversion occurred in the Si and these events can thus be singled out). Double-sided Si is thus superior to two single-sided Si layers of half thickness, as all Si events will have both coordinates. In essence, this explains why the modulation does not change when the two Si planes are replaced with one double-side plane of same thickness. The same amount of useful Si events will be collected in both cases. If the conversion foils are made thinner, however, Si events cease to dominate the polarization signal, and double-sided Si planes do improve the modulation, by almost 50 % when $\tau = 0.02$. As discussed previously, the critical energy where the Compton cross section is equal to the pair production cross section is proportional to $1/Z$, and for Si half the events are Compton events at 12 MeV; at energies lower than 30 MeV, Si events are thus contaminated by Compton events.

What do these results mean for observations of polarized pulsar emission? If no model is assumed, the observed γ -ray pulse must be divided into several phase bins to map the position angle variations as a function of phase. Simple models of the γ -ray pulsar emission processes predict large polarizations of ~ 80 %. At the opposite extreme, polarization may be as low as observed in the optical, or 20 %. Adopting this pessimistic view, observations of the polarization seep would be challenging. Combining the realistic improvements to *GLAST*, thin $\tau = 0.02$ conversion foils and double-sided Si layers, three years of

Vela data would be needed for six such 3σ measurements. Clearly, this is at the limit of what is possible. On the other hand, 80 % polarized flux from Vela could be detected with 3σ significance in two weeks. At a minimum, *GLAST* will thus be able to rule out models that predict a high degree of linear polarization. Furthermore, additional improvements to *GLAST* are possible. With no x/y ambiguities for instance, the required exposure is reduced by almost half (for $\tau = 0.02$). More than a factor two difference remains between the single foil results and those for multiple planes; better event reconstruction can reduce this gap. It may also be possible to collect photons of energies somewhat lower than 30 MeV, i.e. in the range 10–30 MeV. Extending the sensitive range of *GLAST* to 10 MeV would essentially double the number of photons collected. Finally, Monte Carlo sums above 30 MeV show moderately improved polarization sensitivity (per photon), so the required exposures may be somewhat shorter.

Polarization measurements are at the opposite extreme to angular resolution in terms of optimizing the tradeoff between detector errors and the number of photons collected. Other physics goals such as the imaging of extended or confused regions have intermediate requirements. Hopefully at this early stage in the design of *GLAST* a suitable optimization of the instrument can be found that will satisfy all the *GLAST* physics goals. Although challenging, polarization measurements *are possible* with an improved *GLAST*. More extensive simulations will clearly be necessary in finding optimal solutions to both the hardware design and event reconstruction issues.

Acknowledgements

This work was supported in part by NASA grants NAGW 2963, NAG 5-2037 and NAG 5-3231. Helpful discussions with Roger W. Romani, Bill Tompkins, T. Burnett and W.B. Atwood are acknowledged. The software and data are available from <http://astro.stanford.edu/home/ion>.

REFERENCES

- Atwood, W.B., *et al.* 1992, *Int. J. of Mod. Phys.*, C3, 459
- Caraveo, P.A., *et al.* 1988, *ApJ*, 327, 203
- Jauch, J.M. and Rohrlich, F. 1975, Springer-Verlag (New York)
- Kel'ner, S.R. *et al.* 1975, *Yad. Fiz.*, 21, 604
- Kotov, Yu.D. 1988, *Space Sci. Rev.*, 49, 185
- Lynch, G.R. and Dahl, O.I. 1991, *Nucl. Instr. and Meth.*, B58, 6
- Mattox, J.R. 1991, *Exp. Astron.*, 2, 75
- Mattox, J.R., *et al.* 1990, *ApJ*, 363, 270
- Maximon, L.C. and Olsen, H. 1962, *Phys. Rev.*, 126, 310
- Romani, R.W. and Yadigaroglu, I.-A. 1995, *ApJ*, 438, 314
- Wick, G.C. 1950, *Phys. Rev.*, 81, 467
- Yang, C.N. 1950, *Phys. Rev.*, 77, 722